



HAL
open science

Glass-forming ability correlated with the liquid-liquid transition in Pd_{42.5}Ni_{42.5}P₁₅ alloy

En-Yi Chen, Si-Xu Peng, Liang Peng, Marco Di Michiel, Gavin B.M. Vaghan, Yao Yu, Hai-Bin Yu, Beatrice Ruta, Shuai Wei, Lin Liu

► **To cite this version:**

En-Yi Chen, Si-Xu Peng, Liang Peng, Marco Di Michiel, Gavin B.M. Vaghan, et al.. Glass-forming ability correlated with the liquid-liquid transition in Pd_{42.5}Ni_{42.5}P₁₅ alloy. *Scripta Materialia*, 2021, 193, pp.117-121. 10.1016/j.scriptamat.2020.10.042 . hal-03093637

HAL Id: hal-03093637

<https://hal.science/hal-03093637>

Submitted on 26 Nov 2021

HAL is a multi-disciplinary open access archive for the deposit and dissemination of scientific research documents, whether they are published or not. The documents may come from teaching and research institutions in France or abroad, or from public or private research centers.

L'archive ouverte pluridisciplinaire **HAL**, est destinée au dépôt et à la diffusion de documents scientifiques de niveau recherche, publiés ou non, émanant des établissements d'enseignement et de recherche français ou étrangers, des laboratoires publics ou privés.

1 **Glass-forming ability correlated with the liquid-liquid transition in**
2 **Pd_{42.5}Ni_{42.5}P₁₅ alloy**

3 En-Yi Chen^{1,2}, Si-Xu Peng², Liang Peng^{1,2}, Marco Di Michiel³, Gavin B. M. Vaughan³,
4 Yao Yu^{*1,2}, Hai-Bin Yu², Beatrice Ruta^{3,4}, Shuai Wei⁵, Lin Liu^{*1}

5 ¹State Key Laboratory of Materials Processing and Die & Mould Technology, School of
6 Materials Science and Engineering, Huazhong University of Science and Technology,
7 Wuhan 430074, China.

8 ²Wuhan National High Magnetic Field Center, Huazhong University of Science and
9 Technology, Wuhan 430074, China.

10 ³ESRF—The European Synchrotron, CS40220, Grenoble 38043, France.

11 ⁴Univ Lyon, Université Claude Bernard Lyon 1, CNRS, Institut Lumière Matière,
12 Villeurbanne, France.

13 ⁵I. Institute of Physics (IA), RWTH Aachen University, Aachen 52074, Germany.

14 *Corresponding authors.

15 E-mail: ensiyu@mail.hust.edu.cn (Y.Y.); lliu2000@mail.hust.edu.cn (L.L.)

16 **Abstract**

17 Alloy melts can solidify into metallic glasses if cooled fast enough to avoid crystallization.
18 Glass-forming ability (GFA), a measure of the ease of vitrification, is vital for the
19 fundamental understanding of glass formation, and is also crucial for the application of
20 metallic glasses. Previous studies of GFA mainly focused on the undercooled liquid phase,
21 while the influence of the evolution of the stable melts on GFA is rarely addressed. Here
22 we show that the Pd_{42.5}Ni_{42.5}P₁₅ glass-forming liquid, in which a first-order liquid-liquid
23 transition (LLT) takes place at $T_{LL} = 1063$ K high above its liquidus temperature, shows
24 significantly different GFA when quenched from the temperature above or below T_{LL} .
25 Moreover, the pathway and kinetics of crystallization of the melt are strongly related to the

26 kinetics of the LLT. Our work provides new insights into the vitrification process and the
27 kinetics of crystallization, and contributes to designing more stable metallic glasses.

28 **Keywords**

29 Crystallization, Phase transformation kinetics, Metallic glass, Time-temperature-
30 transformation, Nuclear magnetic resonance

31

32 The unsatisfactory glass-forming ability is a major bottleneck of the structural
33 application of metallic glasses even though they show superior mechanical properties [1,
34 2]. Over the past half century, profound studies bring a series of breakthroughs in GFA of
35 metallic glass, which also deepen the fundamental understanding of the glass formation
36 and crystallization process [3-5]. As the formation of glass is a competing process between
37 supercooled liquid and crystalline phases, the understanding of GFA is mainly examined
38 through the lens of classical nucleation theory (CNT), where GFA is related to the crystal
39 nucleation rate per unit volume, I_n , and low nucleation rate means good GFA [6-10]. Here
40 I_n is expressed as $I_n = \frac{A_v}{\eta(T)} \exp\left(-\frac{16\pi\sigma^3}{3k_B T [\Delta g(T)]^2}\right)$, where A_v is a constant, $\eta(T)$ is the
41 viscosity of undercooled liquid, σ is the interfacial energy between liquid and nuclei and
42 $\Delta g(T)$ is the free energy difference between liquid and crystalline phases. Therefore, the
43 evolution of the supercooled liquid and the differences between the supercooled liquid and
44 crystalline phases are commonly believed to be the most important factors affecting GFA
45 [7, 11]. However, growing evidences of multistep nucleation with much higher nucleation
46 rate contradict the basic assumption of CNT, suggesting that the CNT encounters some
47 limitations in the interpretation of the kinetics and pathway of crystallization [12-16].
48 These limitations strongly indicate that the current understandings of GFA are far from
49 comprehensive. Recently, more factors have been taken into consideration [17-20], while
50 there are still many issues about GFA which are not well understood.

51 Among all the factors that may affect GFA, the evolution of the alloy melt above its
52 liquidus temperature T_{liq} is the least considered. The main reason is that the equilibrium
53 melt is commonly thought as a simple liquid with a very short ($\sim 10^{-13}$ s) relaxation time.
54 It seems impossible that the changes in the melt above T_{liq} could affect the behaviors of
55 undercooled liquid, let alone the crystallization process [21]. Thus, it is commonly accepted
56 that the GFA is irrelevant to the state of equilibrium melt.

57 However, the situation could be quite different for the alloy melt with a liquid-liquid
58 transition taking place above T_{liq} . Contrary to the conventional understanding, this melt is
59 very complex, and exhibits two distinct liquid phases [22]. In addition, the transition
60 between the two liquids shows the characteristics of first-order phase transition, which

61 implies that both liquid states could be undercooled to the temperature far below T_{liq} , even
62 approaching the glass transition temperature T_g . Consequently, the influences of the
63 complexity of the alloy melts together with the kinetics of the first-order LLT should be
64 taken into consideration on the GFA of the melts.

65 Herein, a glass-forming alloy of $\text{Pd}_{42.5}\text{Ni}_{42.5}\text{P}_{15}$ is selected, and the influence of LLT on
66 its GFA is studied. The liquidus temperature of the $\text{Pd}_{42.5}\text{Ni}_{42.5}\text{P}_{15}$ system was determined
67 as 993 K by the flash differential scanning calorimetry (FDSC) (Fig. S1). In situ ^{31}P high-
68 temperature nuclear magnetic resonance (NMR) was carried out to characterize the LLT
69 above T_{liq} . Firstly, step cooling experiments were conducted, in which the $\text{Pd}_{42.5}\text{Ni}_{42.5}\text{P}_{15}$
70 alloy was first heated to 1293 K and held there for 30 min for homogenization, and then it
71 was cooled step by step to 993 K with 40 K interval in the range of 1293 ~ 1093 K and 20
72 K interval below 1053 K. NMR spectra were taken isothermally after equilibrating for 30
73 min at each step. The peak position of each spectrum, the Knight shift (K_s), which is
74 determined by the ensemble average of local magnetic field around ^{31}P nuclei and sensitive
75 to the changes in structure [22, 23], is plotted in Fig. 1a as a function of temperature (T).
76 K_s varies linearly above 1063 K with a slope of -0.03 ppm/K (red line), but with a slope of
77 1.73 ppm/K (pink line) below 1063 K, indicating a significant change in the P-centered
78 local structures. This result implies that an LLT may take place at $T_{\text{LL}} = 1063$ K. Two
79 typical ^{31}P spectra above and below T_{LL} are shown in the insets of Fig. 1a. Each spectrum
80 is a single Lorentzian peak and the integral areas of the peaks remain identical, indicating
81 that the system above or below T_{LL} is a homogeneous liquid without any loss of the
82 contributing P atoms.

83 In an ideal metallic liquid, the magnetic coupling between nuclei and s -like conduction
84 electrons through the Fermi contact interaction is the dominant mechanism of both Knight
85 shift and spin-lattice relaxation, leading to the Korringa relation $TT_1K_s^2 = \frac{\hbar\gamma_e^2}{4\pi k_B\gamma_n^2} f$, where
86 T_1 is the spin-lattice relaxation time (Fig. S2), γ_e and γ_n are respectively the electron and
87 nucleus gyromagnetic ratio, \hbar and k_B are respectively the reduced Planck and Boltzmann
88 constant, and f is a constant related to the electron-electron interaction [24-26]. Thus, the
89 value of $TT_1K_s^2$ is supposed to be a constant. However, in the presence of strong covalent

90 bonds, the electrons tend to be localized, remaining in the vicinity of nuclei for longer time,
91 and thus the spin-lattice relaxation process would be more efficient. Therefore, the actual
92 relaxation time T_1 is shorter compared with the case in ideal metallic liquid, leading to the
93 breakdown of Korringa relation [27, 28]. Fig. 1b plots the value of $TT_1K_s^2$ versus T , which
94 is almost constant above 1063 K, but drops substantially below 1063 K with decreasing
95 temperature, indicating the breakdown of Korringa relation. This result suggests that the
96 covalent bonding in the liquid is significantly enhanced below 1063 K, which could be the
97 structural origination of the LLT.

98 Further, the kinetics associated with the LLT was examined. The sample was heated to
99 1173 K and held there isothermally for 30 min, and then fast cooled to one of the
100 undercooled temperature (with respective to $T_{LL} = 1063$ K) $T_{iso} = 1055, 1053, 1050, 1047,$
101 $1045,$ and 1043 K in about 1.5 min, and held there isothermally. Once the temperature
102 stabilized at each T_{iso} , NMR spectra were recorded every 10 s to monitor any possible
103 transition. Fig. 1c shows the measured K_s at different T_{iso} . When reaching T_{iso} , K_s initially
104 follows the linear extrapolation (red line) of the T -dependent K_s above 1063 K measured
105 in the step cooling experiments. After a certain incubation time τ , K_s starts to jump to the
106 expected value determined by the linear fit of the T -dependent K_s below 1063 K (pink line).
107 These results clearly show that the stable liquid above 1063 K (high-temperature liquid,
108 named as HTL) can be undercooled below T_{LL} and finally transforms to the stable liquid
109 below 1063 K (low-temperature liquid, named as LTL). Such behavior is consistent with
110 the first-order phase transition [29]. The average incubation time τ of three independent
111 measurements at each temperature versus the degree of undercooling $\Delta T = T_{LL} - T_{iso}$ is
112 shown in Fig. 1d. As ΔT increases from 8 to 20 K (i.e., T_{iso} decreases from 1055 to 1043
113 K), the incubation time decreases rapidly from 240 s to 30 s. The inset shows the plot of
114 $\log(T_{iso} / \tau)$ versus $\log(\Delta T)$, which can be well fitted with a linear function, indicating a
115 power-law relation of $\tau \propto T_{iso} / (\Delta T)^m$ with $m = 2.1$. Similar power-law was also observed
116 in the LLTs in $\text{La}_{50}\text{Al}_{35}\text{Ni}_{15}$ liquid [22] and molten sodium acetate trihydrate [30].

117 To further explore the difference between HTL and LTL, two glassy samples, labeled as
118 HTA and LTA accordingly, were prepared by quenching the melt from 1223 K (above T_{LL})

119 and 1023 K (below T_{LL}) using melt-spinning technique, respectively. High-energy
120 synchrotron X-ray diffraction (XRD) was then employed to examine the structure of the
121 two glassy samples. As shown in Fig. 2a, no sharp Bragg peaks corresponding to any
122 crystallites are detected on the structure factors $S(q)$, confirming the amorphous nature of
123 the two samples. These results are consistent with the high-resolution transmission electron
124 microscopy (HRTEM) results (Fig. S3). The full width at half maximum (FWHM) of the
125 first peak in $S(q)$ are about 0.44 \AA^{-1} and 0.34 \AA^{-1} for HTA and LTA, respectively. The
126 narrower FWHM of LTA suggests the existence of more ordered structures in this glass.
127 The structural details can be better appreciated from real space analysis by looking at the
128 pair correlation function $G(r)$ obtained by the Fourier transformation of the corresponding
129 $S(q)$ (Fig. 2b). The positions difference of the first maxima of $G(r)$ is very subtle (2.75 \AA
130 for LTA and 2.74 \AA for HTA). The increased order in the structure of the LTA is reflected
131 in well-defined oscillations up to the 12th shell in the LTA while only up to the 8th shell in
132 the HTA. This behavior is clearly identified from the difference in $G(r)$ between HTA and
133 LTA, obtained by subtracting the former from the latter (inset of Fig. 2b). The difference
134 between these two $G(r)$ curves are negligible up to the second minimum distance ($r < 5.9$
135 \AA), but beyond this distance, LTA shows an enhanced correlation which is still pronounced
136 even up to $r > 25 \text{ \AA}$. These results suggest that the structure of short-range clusters in LTA
137 and HTA are almost the same, but a more pronounced medium-range ordering presents in
138 LTA.

139 LLTs were supposed to take place in several metallic glass-forming liquids, but the
140 structural mechanism associated with the LLT was not clear [31-33]. NMR observables are
141 sensitive to the interaction between electrons and nuclei, and can provide information of
142 all nearest-neighbor atoms surrounding the atom and possibly beyond. Combined with the
143 evidence of synchrotron XRD, more detailed structural changes can be revealed. Since the
144 glass is commonly considered as “frozen liquid”, the results of HTA and LTA imply that
145 the structures of short-range clusters in LTL and HTL could be almost identical, but the
146 correlation between the short-range clusters in LTL and HTL should be different. Recalling
147 the significantly enhanced covalent bonding in LTL suggested by the breakdown of
148 Korringa relation (Fig. 1b), it is reasonable to assume that the transition from HTL to LTL

149 is associated with the increase of the short-range clusters and stronger correlation between
150 the clusters, consistent with the two-order-parameter model [34, 35].

151 The GFA of the two liquids were examined by FDSC experiments through measuring
152 the critical cooling rate R_c , which is the slowest cooling rate at which equilibrium liquid
153 can be quenched into glass without detectable crystallites, and a lower R_c stands for a better
154 GFA [36, 37]. The sample was first heated to a predetermined temperature $T_q = 1073$ (i.e.,
155 10 K above T_{LL}) at a constant rate of 100 K/s and kept there isothermally for 30 s, then
156 cooled to room temperature at a series of cooling rate q^- (50 ~ 40000 K/s) to obtain samples
157 with different content of amorphous phase. After this pretreatment, the contents of
158 amorphous phase in these samples were measured by FDSC via heating each sample from
159 room temperature to 1073 K at a constant rate of 100 K/s (see the inset of Fig. 3a for
160 temperature protocol). For comparison, these procedures were repeated for $T_q = 1023$ K
161 (i.e., 40 K below T_{LL}). Fig. 3a shows a representative DSC heating curve for the sample
162 obtained from $T_q = 1073$ K and $q^- = 40000$ K/s. The two exothermic peaks (around 685 K
163 and 770 K) are related to the polyamorphic transition [38, 39] and the crystallization of the
164 amorphous phase, respectively, and the endothermic peaks (around 880 K) represent the
165 melting process. Fig. 3b plots the area of the second exothermic peak (ΔH) versus T . Here,
166 ΔH of each sample was normalized to that of the sample obtained from $T_q = 1073$ K and
167 $q^- = 40000$ K/s (this sample was used as the reference because it is fully amorphous, see
168 the discussion below), and this value is directly proportional to the content of amorphous
169 phase in each sample. For samples cooled from $T_q = 1023$ K (i.e., from LTL), the content
170 of amorphous phase does not change when $q^- > 6000$ K/s, but drops significantly when q^-
171 < 6000 K/s, suggesting that R_c is about 6000 K/s for LTL. However, for samples cooled
172 from $T_q = 1073$ K (i.e., from HTL), the content of amorphous phase remains constant until
173 $q^- < 100$ K/s, indicating that R_c is about 100 K/s for HTL. The results demonstrate clearly
174 that HTL exhibits much better GFA compared to LTL.

175 The significance of the current experiments is that the GFA is observed to be closely
176 related to the liquid-liquid transition event. It is shown unambiguously that an alloy melt
177 can exhibit two significantly different GFA without change in composition. Due to the
178 first-order nature of the LLT, both HTL and LTL can be maintained to the temperature far

179 below T_{liq} , and further vitrified into different glasses (Fig. 2a). The evolutions of the two
180 liquids are schematically shown in Fig. 4a. As HTL and LTL are distinct liquid states, it is
181 reasonable that they show different crystallization kinetics and hence different GFAs.

182 The LLT plays a crucial role in the crystallization of HTL. On the one hand, it provides
183 an alternative crystallization pathway for HTL. The crystallization of HTL would follow
184 one of the two possible pathways: either crystallize directly from HTL state (Path I in Fig.
185 4a), or crystallize via LTL after the LLT takes place (Path II in Fig. 4a). In the latter case,
186 the supercooled LTL acts as an intermediate state between the supercooled HTL and
187 crystalline state. The existence of Path II is coincident with previous studies [38, 39], where
188 it was suggested that the HTA transformed firstly to a supercooled liquid (supercooled
189 liquid I) above its glass transition temperature, and then to another supercooled liquid
190 (supercooled liquid II) before crystallization upon further heating. Although the
191 supercooled liquid I and II are not cognized in detail, they are consistent with the
192 supercooled HTL and LTL in our picture shown in Fig. 4a, respectively. Thus, our
193 experiments suggest a new possible crystallization pathway upon cooling, i.e., crystallize
194 via an intermediate liquid state (Path II).

195 On the other hand, the LLT may also change the crystallization kinetics of HTL. The
196 selection of the crystallization pathway is determined by the competition between the
197 kinetics of LLT and the crystallization kinetics of HTL. Once the incubation time of LLT
198 is shorter than that of the crystallization of HTL, HTL would crystallize through Path II.
199 Fig. 4b schematically shows a possible relationship between the crystallization time-
200 temperature-transformation (TTT) curves of HTL (green dashed line) and LTL (red line),
201 together with the TTT curve of LLT (cerulean line). Here, the critical cooling rate of HTL,
202 R_c^{HTL} , is no longer related to the intrinsic TTT curve of HTL, but related to the effective-
203 TTT curve (dark dotted line), which is the superposition of the TTT curve of LLT and the
204 crystallization TTT curve of LTL, with its nose point around the lower intersection of the
205 two curves. The minimum cooling rate to bypass this effective-TTT curve can be
206 determined as $R_c = (T_{LL} - T_{en}^{HTL}) / t_{en}^{HTL}$, where T_{en}^{HTL} and t_{en}^{HTL} are the temperature and time
207 scale at the nose point. By assuming that T_{en}^{HTL} is around the nose temperature T_n^{LTL} of the

208 TTT curve of LTL, which can be estimated as $T_n^{\text{LTL}} = T_g + 0.5(T_{\text{liq}} - T_g) = 780 \text{ K}$ [40] and
209 $t_{\text{en}}^{\text{HTL}}$ deduced from the continuous-cooling-transformation (CCT) curve of LLT
210 constructed by the method developed by Grange and Keifer [41], is about 1.4 s (Fig. S4),
211 R_c can be roughly estimated as 200 K/s. To our great surprise, this value is very close to
212 the R_c^{HTL} acquired from the FDSC experiments. This result strongly indicates that the
213 picture described in Fig. 4b could be the case of the crystallization in $\text{Pd}_{42.5}\text{Ni}_{42.5}\text{P}_{15}$.

214 It is of interest to note that HTL exhibits a better GFA than LTL. Although the detailed
215 kinetics of the direct crystallization process of HTL is experimentally unachievable due to
216 the interference of LLT, it can be concluded qualitatively from the poor GFA of LTL that
217 the crystal nucleation rate per unit volume I_n from LTL should be much higher than that
218 from HTL. This may result from the formation of the clusters with medium-range ordering
219 in the supercooled LTL, and such clusters may act as precursors for the nucleation of the
220 crystalline phase [11], reducing the interfacial energy σ and leading to a lower energy
221 barrier for the formation of the crystal nuclei and hence the poor GFA of LTL.

222 In summary, our in situ high-temperature NMR studies show that the glass-forming
223 liquid $\text{Pd}_{42.5}\text{Ni}_{42.5}\text{P}_{15}$ presents a first-order LLT at the temperature of 1063 K, high above
224 the liquidus temperature of 993 K, accompanied by a drastic enhancement of the covalent
225 bonding below 1063 K. The two liquids can be vitrified into two corresponding glasses
226 which are different in the medium-range ordering rather than the structure of short-range
227 clusters. These results suggest that the LLT may be a result of the increase of the short-
228 range clusters. The FDSC studies reveal that the high-temperature liquid exhibits much
229 better GFA than the low-temperature liquid, which may be ascribed to the enhancement of
230 medium-range ordering in the supercooled LTL. Further analyses indicate that the LLT can
231 provide an indirect crystallization pathway for HTL, and moreover, the kinetics of LLT
232 has a significant influence on the GFA. This effects of LLT provides a new way for future
233 study of the process of crystallization and is also important for the fabrication of metallic
234 glasses. What is more, our work may also provide an alternative understanding for some
235 traditional phenomena. For instance, many metallic glass-forming liquids exhibit
236 overheating effects, where the nucleation behavior of the system or the mechanical
237 properties of the metallic glasses show markedly difference with different overheating

238 temperature [42, 43]. Till now, there are only qualitative understandings for these
239 phenomena. It is proposed to be related to the heterogeneities in the liquid, which dissolve
240 above a threshold temperature. However, such behavior could be quantitatively explained
241 within our LLT scenario, where T_{LL} is the threshold temperature.

242

243

244 **Declaration of Competing Interest**

245 The authors declare that they have no known competing financial interests or personal
246 relationships that could have appeared to influence the work reported in this paper.

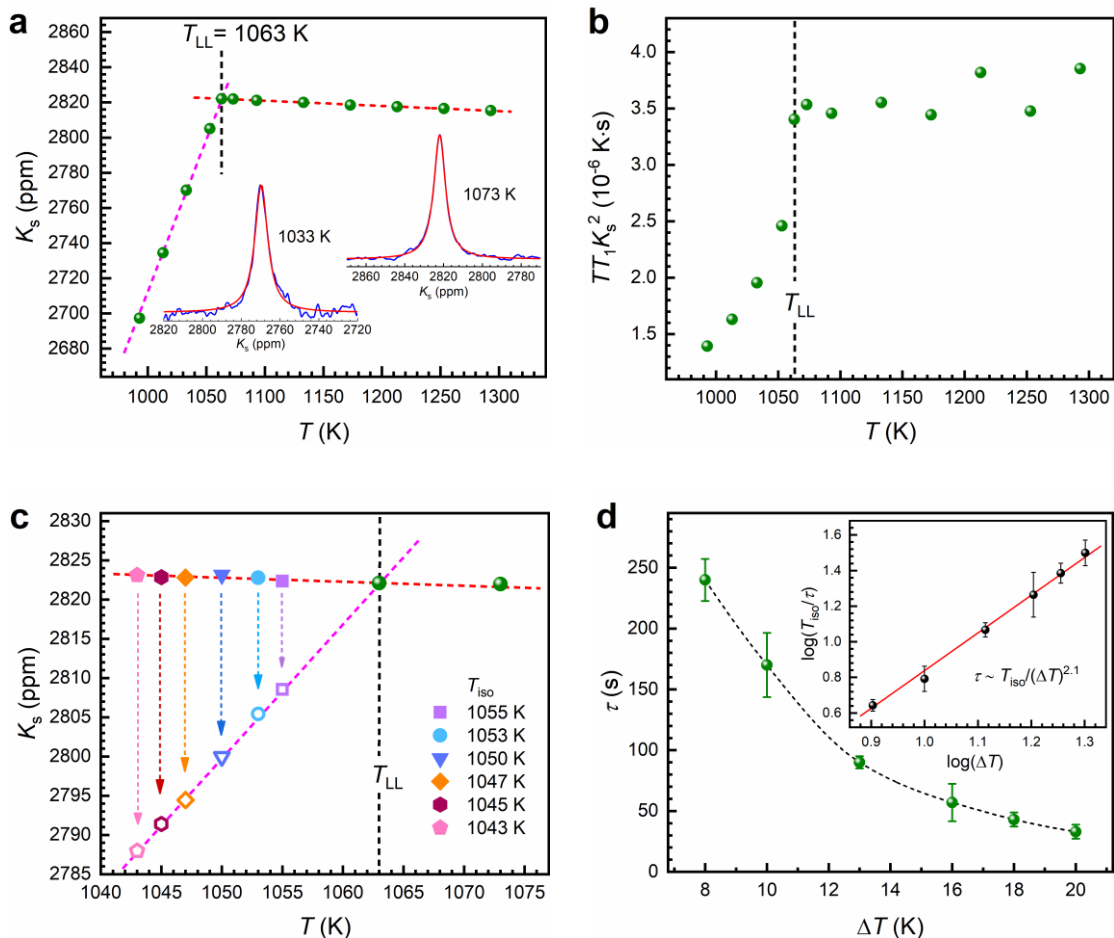
247 **Acknowledgement**

248 The authors are grateful to the Analytical and Testing Center of HUST for technical
249 assistance. This work was financially supported by the National Natural Science
250 Foundation of China (Grant No. 51872105).

251 **References**

- 252 [1] W.H. Wang, C. Dong, C.H. Shek, *Mater. Sci. Eng. R Rep.* 44(2) (2004) 45-89.
253 [2] M. Telford, *Mater. Today* 7(3) (2004) 36-43.
254 [3] A.L. Greer, *Science* 267(5206) (1995) 1947.
255 [4] Y. Li, Q. Guo, J.A. Kalb, C.V. Thompson, *Science* 322(5909) (2008) 1816.
256 [5] C.G. Tang, P. Harrowell, *Nat. Mater.* 12(6) (2013) 507-511.
257 [6] M.H. Cohen, D. Turnbull, *J. Chem. Phys.* 31(5) (1959) 1164-1169.
258 [7] D. Turnbull, *Contemp. Phys.* 10(5) (1969) 473-488.
259 [8] A. Inoue, *Acta Mater.* 48(1) (2000) 279-306.
260 [9] Z.P. Lu, C.T. Liu, *Acta Mater.* 50(13) (2002) 3501-3512.
261 [10] D.M. Herlach, *Mater. Sci. Eng. R Rep.* 12(4) (1994) 177-272.
262 [11] J. Russo, F. Romano, H. Tanaka, *Phys. Rev. X* 8(2) (2018) 021040.
263 [12] D. Erdemir, A.Y. Lee, A.S. Myerson, *Acc. Chem. Res.* 42(5) (2009) 621-629.
264 [13] P.G. Vekilov, *Cryst. Growth Des.* 10(12) (2010) 5007-5019.
265 [14] J. De Yoreo, *Nat. Mater.* 12(4) (2013) 284-285.
266 [15] J. Lee, J. Yang, S.G. Kwon, T. Hyeon, *Nat. Rev. Mater.* 1(8) (2016) 16034.
267 [16] J.J. De Yoreo, P.U.P.A. Gilbert, N.A.J.M. Sommerdijk, et al., *Science* 349(6247)
268 (2015) aaa6760.
269 [17] P. Zalden, F. Quirin, M. Schumacher, et al., *Science* 364(6445) (2019) 1062.
270 [18] S. Wei, G.J. Coleman, P. Lucas, C.A. Angell, *Phys. Rev. Appl* 7(3) (2017) 034035.
271 [19] J. Schroers, W.L. Johnson, *J. Appl. Phys.* 88(1) (2000) 44-48.

- 272 [20] J. Schroers, Y. Wu, R. Busch, W.L. Johnson, *Acta Mater.* 49(14) (2001) 2773-2781.
273 [21] A. Cavagna, *Phys. Rep.* 476(4) (2009) 51-124.
274 [22] W. Xu, M.T. Sandor, Y. Yu, et al., *Nat. Commun.* 6 (2015) 7696.
275 [23] L.L. Li, J. Schroers, Y. Wu, *Phys. Rev. Lett.* 91(26) (2003) 265502.
276 [24] A. Abragam, *Principles of Nuclear Magnetism*, Clarendon Press, Oxford, 1961.
277 [25] C.P. Slichter, *Principles of Magnetic Resonance*, Harper & Row Publishers, New
278 York, 1963.
279 [26] J. Koringa, *Physica* 16(7) (1950) 601-610.
280 [27] W.W. Warren, *Phys. Rev. B* 3(11) (1971) 3708-3724.
281 [28] R. Dupree, D.J. Kirby, W. Freyland, *Philos. Mag. B* 46(6) (1982) 595-606.
282 [29] D. Turnbull, *Solid State Physics*, Elsevier 1956, pp. 225-306.
283 [30] X. Liu, S.Y. Liu, E.Y. Chen, et al., *J. Phys. Chem. Lett.* 10(15) (2019) 4285-4290.
284 [31] C. Way, P. Wadhwa, R. Busch, *Acta Mater.* 55(9) (2007) 2977-2983.
285 [32] S. Wei, F. Yang, J. Bednarcik, et al., *Nat. Commun.* 4 (2013) 2083.
286 [33] M.E. Blodgett, T. Egami, Z. Nussinov, K.F. Kelton, *Sci. Rep.* 5(1) (2015) 13837.
287 [34] H. Tanaka, *Phys. Rev. E* 62(5) (2000) 6968-6976.
288 [35] H. Tanaka, *Eur. Phys. J. E* 35(10) (2012) 113.
289 [36] C.S. Ray, S.T. Reis, R.K. Brow, et al., *J. Non-Cryst. Solids* 351(16) (2005) 1350-
290 1358.
291 [37] Q.J. Zheng, Y.F. Zhang, M. Montazerian, et al., *Chem. Rev.* 119(13) (2019) 7848-
292 7939.
293 [38] S. Lan, Y. Ren, X.Y. Wei, et al., *Nat. Commun.* 8 (2017) 14679.
294 [39] Q. Du, X.J. Liu, H.Y. Fan, et al., *Mater. Today* 34 (2020) 66-77.
295 [40] Z.P. Lu, C.T. Liu, *Phys. Rev. Lett.* 91(11) (2003) 115505.
296 [41] R. Grange, J. Kiefer, *Trans. ASM* 29(1) (1941) 85.
297 [42] S. Mukherjee, Z. Zhou, J. Schroers, et al., *Appl. Phys. Lett.* 84(24) (2004) 5010-
298 5012.
299 [43] Y. Zhao, S. Kou, H. Suo, et al., *Mater. Des.* 31(2) (2010) 1029-1032.
300

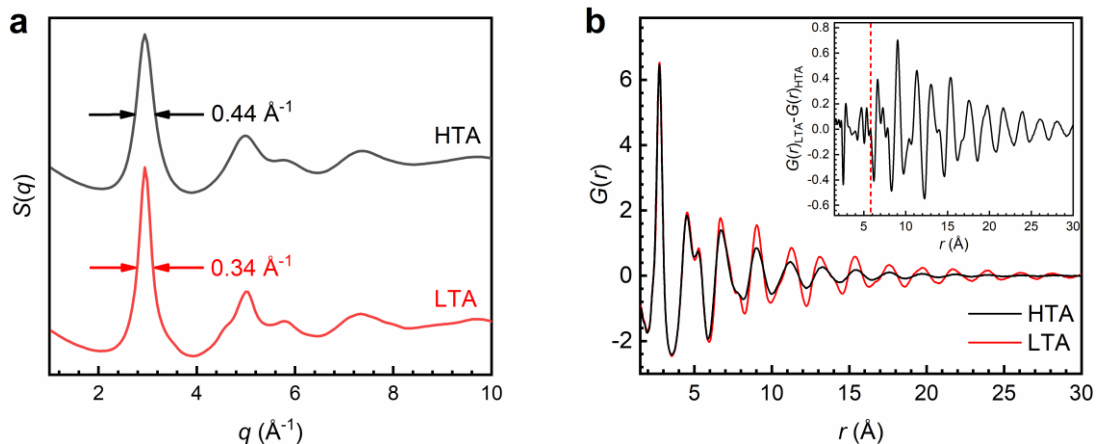


301

302

303 **Fig. 1.** Liquid-liquid transition in the equilibrium $\text{Pd}_{42.5}\text{Ni}_{42.5}\text{P}_{15}$ melt characterized by
 304 NMR. (a) Temperature dependence of ^{31}P Knight shift (K_s). The two linear fits (red and
 305 pink dashed lines) intersect at 1063 K. The insets are two typical spectra (blue line) above
 306 and below the transition temperature with the Lorentzian fitting of the spectrum (red line).
 307 (b) Value of $TT_1K_s^2$ as a function of temperature. (c) The changes of K_s at different
 308 undercooled temperatures T_{iso} after quenching the melt from 1173 K. The solid and open
 309 symbols represent the initial and equilibrium K_s , respectively. (d) The average incubation
 310 time τ versus degree of undercooling $\Delta T = 1063 - T_{\text{iso}}$. The inset plots $\log(T_{\text{iso}}/\tau)$ versus
 311 $\log(\Delta T)$ and the slope of the linear fit is 2.1.

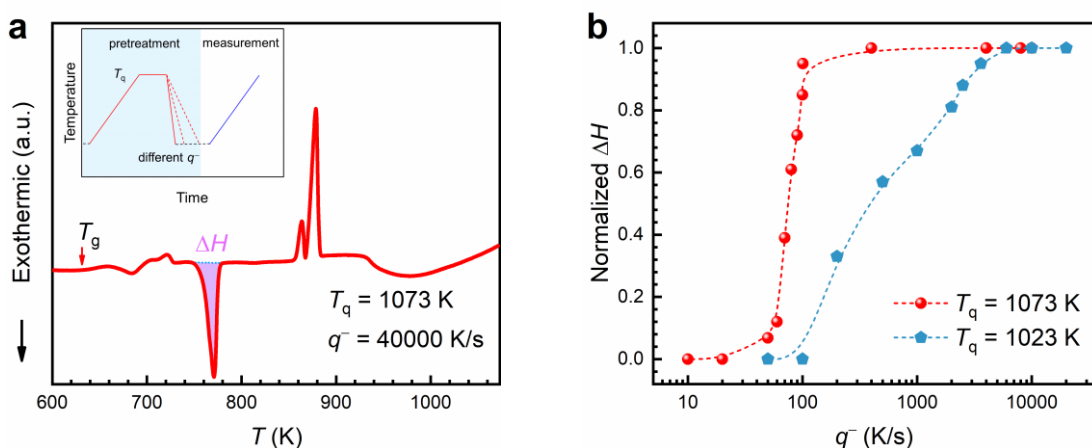
312



313

314 **Fig. 2.** Structural difference of HTA and LTA characterized by high-energy synchrotron
 315 XRD. (a) Structure factors $S(q)$ of HTA and LTA. (b) Pair correlation functions $G(r)$ of
 316 HTA and LTA. The inset shows the difference in $G(r)$ between LTA and HTA.

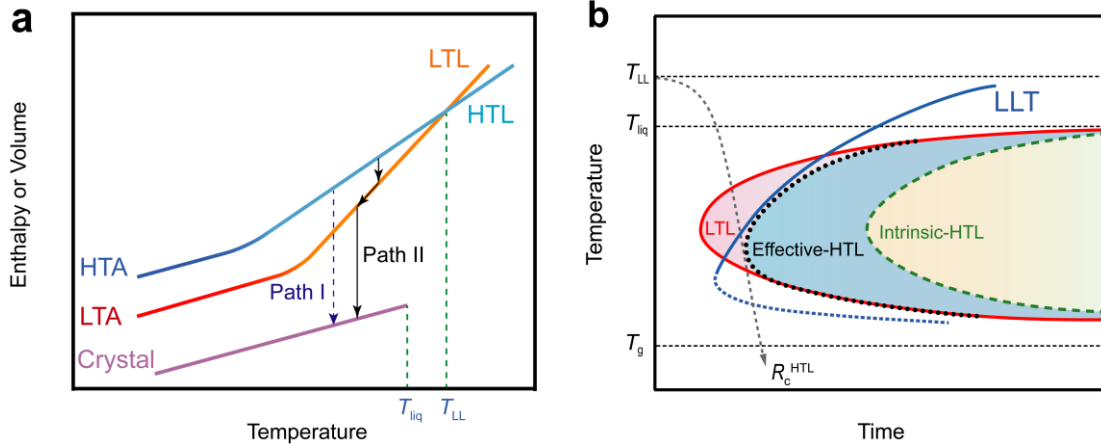
317



318

319 **Fig. 3.** Glass-forming ability of the two liquids characterized by FDSC. (a) A typical FDSC
 320 heating curve of the sample obtained from $T_q = 1073$ K and $q^- = 40000$ K. The enthalpy of
 321 crystallization is denoted as ΔH . The inset shows the temperature protocol of the FDSC
 322 experiments. (b) The content of amorphous phase as a function of cooling rate q^- of the
 323 samples obtained from $T_q = 1073$ K and 1023 K, respectively.

324



325

326 **Fig. 4.** Effects of LLT on the pathways and kinetics of crystallization. (a) Schematic
 327 evolution of enthalpy or volume upon cooling the melt. (b) Mechanism of the different
 328 GFA of HTL and LTL. The red and green dashed lines represent the intrinsic crystallization
 329 TTT curve of LTL and HTL, respectively. The cerulean line represents the TTT curve of
 330 LLT. The TTT curve of LLT intersects the TTT curve of LTL at high and low temperature
 331 and the black dotted line denotes the effective crystallization TTT curve of HTL with its
 332 nose around the low intersection. R_c^{HTL} is the critical cooling rate to bypass the effective
 333 TTT curve of HTL.